JOURNAL OF GUIDANCE, CONTROL, AND DYNAMICS
Vol. 17, No. 6, November–December 1994

Application of Piezoelectric Devices to Vibration Suppression

Chin Chung Won* and Jeffrey L. Sulla†
Lockheed Engineering and Sciences Company, Inc., Hampton, Virginia 23666
and
Dean W. Sparks Jr.‡ and W. Keith Belvin§
NASA Langley Research Center, Hampton, Virginia 23681-0001

Embedded piezoelectric devices may be ideally suited for vibration control of space structures, which lack an inertial ground. When subjected to an input voltage, an embedded piezoelectric actuator changes its dimensions, which in turn generates a pair of forces exerted on adjacent structural members. From the direct piezoelectric effect, an embedded piezoelectric transducer generates an electric charge proportional to the structural dynamic response. In this paper, the implementation, testing, and modeling of an active truss structure with piezoelectric sensors and actuators are described. Linear quadratic Gaussian, second-order, and direct-rate feedback control schemes are designed to suppress the vibrations of the active structure. Simulation and test results are presented. It is shown that special model reduction considerations are required to achieve good correlation between test and analysis.

Nomenclature

The typical symbology for piezoelectric material properties are used in this paper. Except where noted, the piezoelectric variables are with respect to the standard piezoelectric material 1-2-3 Cartesian coordinate frame. The single, or first of the double, subscript denotes the direction of the applied/sensed electrical field. The second subscript represents the direction of the stress/strain in the piezoelectric material. The subscript r represents the radial direction, as measured in a cylindrical coordinate frame.

A = cross-sectional area
$\boldsymbol{A}_c$ = controller state matrix
A_s = surface area
$\boldsymbol{B}, \boldsymbol{B}_i$ = input matrix, ith input matrix
$\boldsymbol{B}_c$ = controller input matrix
$\boldsymbol{C}, \boldsymbol{C}_i$ = output matrix, ith output matrix
$\boldsymbol{C}_c$ = controller output matrix
C^S = total capacitance of piezoceramic stack measured at constant strain
c_{33}^D = elastic modulus measured at constant electric displacement
c_{33}^E = elastic modulus measured at constant electric field
$\boldsymbol{D}$ = damping matrix
$\boldsymbol{D}_c$ = controller direct transmission matrix
D_3, D_r = electric displacement
d = thickness of piezoceramic
E_3, E_r = electric field
e_{33}, e_{31} = piezoelectric stress/electrical field constants
e_{r3} = piezoelectric stress/electrical field constant, radial coordinate
$\boldsymbol{f}$ = input vector
$\boldsymbol{G}$ = constant-gain diagonal matrix
h_{33} = piezoelectric force/charge constant
$\boldsymbol{I}$ = identity matrix
$\boldsymbol{K}$ = stiffness matrix
K^E = elastic stiffness
k = kth digital computer sample
L = length of piezoelectric strut
L_f = length of piezoelectric film
$\boldsymbol{M}$ = mass matrix
m = mass per unit length
N_3 = axial force
n = number of layers of piezoceramics in one piezoelectric strut
Q_3, Q_r = total electric charge
r = radial direction in cylindrical coordinate frame
S_3 = normal strain
T = kinetic energy
T_3 = normal stress
t = time
$\boldsymbol{u}$ = controlled input vector
V = internal energy
V_3 = electric potential difference
W = work done
w = mechanical displacement
w_i = ith nodal displacement
$\boldsymbol{x}$ = state vector
$\boldsymbol{x}_c$ = controller state vector
$\boldsymbol{y}$ = output vector
Z = impedance of current amplifier
z = axis parallel to longitudinal axis of piezoelectric stack
$\boldsymbol{\alpha}$ = diagonal constant matrix
β_{33}^S = dielectric impermeability measured at constant strain
ΔL = elongation
ϕ_{si} = ith static displacement shape
ϕ_{vi} = ith vibrational mode shape
Ω = volume
$(\bullet)_{,z}$ = derivative of variable with respect to z
$(\dot{\bullet})$ = time derivative of variable
$(\bar{\bullet})$ = applied load variable

Received June 19, 1992; presented as Paper 92-4610 at the AIAA Guidance, Navigation, and Control Conference, Hilton Head, SC, Aug. 10–12, 1992; revision received Dec. 20, 1993; accepted for publication Dec. 22, 1993.

*Principle Engineer. Member AIAA.
†Senior Engineer.
‡Aerospace Technologist, GCD Division.
§Aerospace Technologist, SDyD Division. Senior Member AIAA.

Introduction

FUTURE "truss-type" space structures are expected to grow ever larger to meet mission requirements. As a space structure grows larger, the ability to separate the system's operational bandwidth from the spacecraft's structural bandwidth decreases. A result of this crossover in bandwidth is the control/structure interaction (CSI) problem, in which the platform's structural modes interfere with the science instrumentation/mission requirements.

To apply electromechanical forces to a truss structure, an effective method is to replace a truss member or a strut by a piezoelectric

element. This piezoelectric strut works as a load-carrying member as well as a force actuator. A piezoelectric actuator can consist of a stack of piezoceramic disks with the electrical circuit connected in parallel. An embedded piezoelectric element can also be used as a sensor. In this case, the piezoelectric element generates a voltage due to applied strain.

In this paper, the application of piezoelectric actuators and sensors to vibration suppression of a truss structure is studied. Piezoelectric films and strain gauges are used as the control sensors. For active control, linear quadratic Gaussian (LQG) and second-order controllers are designed and compared with direct-rate feedback to validate the modeling and control schemes. The frequency response functions of the analytical model are compared with experimental data. Prediction of the closed-loop time responses are verified by the experimental data. The paper presents strut modeling approaches, a testbed description, finite element modeling issues, and finally closed-loop analytical and test results.

Modeling

For a piezoelectro-elastic body, components of elastic strain and stress and electric field and displacement are the dependent field variables. The equations available are the constitutive equations of the piezoelectric material and the system equations, which are equations of motion and Maxwell's equations. The number of equations should match the number of unknown variables to solve the electrodynamical problem uniquely when the boundary conditions and initial conditions are imposed. For an electrodynamical problem, the known quantities can be the driving mechanical forces, prescribed displacement boundary conditions, initial displacements, external voltages, or external charges.

For a purely elastic body, the governing equations can be expressed in terms of stresses, called Cauchy's first law of motion, or in terms of displacements, the displacement equations of motion.[1] After the stresses (strains) are solved from Cauchy's first law of motion (displacement equations of motion), the strains (stresses) can be obtained from Hooke's law of the material. In contrast, for a dielectric material, the governing equation can be either Maxwell's second equation, which states that the curl of electric fields is zero in the electrostatic case, or the charge equation of electrostatics, which depicts the conservation of electric charge.[2] Solving the governing equations to yield the electric field, Gauss's law is used to solve the electric displacement, or vice versa. The governing equations of a piezoelectric structure were derived by Holland and Eer Nisse[3] and Tiersten.[4] Their derivations resulted in Cauchy's first law of motion and the charge equation of electrostatics. All the driving forces, such as applied surface tractions, prescribed displacement, external electric potential, and external electric charges, appear as boundary conditions. These two sets of equations are coupled due to the piezoelectric effect.

The governing equations for a composite piezoelectric structure are the same as that of an elastic structure or dielectric material except the constitutive equations for a piezoelectric material are used in place of Hooke's law and Gauss's law in the region of piezoelectric material. For a composite piezoelectric structure, the governing equations were developed for a current source by Ha, Keilers, and Chang[5] and Hagood et al.[6] Their derivations after discretization end up as the displacement equations of motion and charge equation of electrostatics with external forces and applied electric charges on the right-hand side of the equations as the driving forces. Because the external charges depend on the load of the piezoelectric structure system, one cannot specify the external charge by using a voltage source unless the system equations are solved. Their governing equations cannot be applied to the case when voltage sources are used to drive the piezoelectric devices. In the case of applied voltage, the driving forces can be applied either by prescribing the electric potential on the appropriate boundaries, as done by Tiersten, or by formulating the problem in terms of mechanical and electric displacements, with the external voltages on the right-hand side of the governing equations as the driving function, as done in Refs. 7 and 8. In this paper, the governing equations for a composite piezoelectric truss structure for voltage sources will be derived using this procedure. Also, for this study, the effects of the bonding layer between the individual piezoelectric materials have been neglected.

To achieve direct-rate feedback control using a piezoelectric actuator, a compatible collocated rate sensor should be used. Although a piezoelectric actuator or sensor covers a finite domain of a continuous structure, the effective force transmission region is concentrated on the edges.[7] After discretization in the spatial domain, the distributed device can usually be approximated as a two-point device in contrast to the one-point actuator (e.g., a shaker) or one-point sensor (e.g., accelerometer). A polyvinylidene fluoride (PVDF) is a compatible piezoelectric sensor with a piezoelectric actuator. A vast study of rate measurements using PVDF films has been conducted by Lee et al.,[9,10] Obal,[11] and Won et al.[7,12] In their studies, the PVDF film generates a signal proportional to strain rate when incorporated with a current amplifier.

Properties

The constitutive equations of a piezoelectric material can be found in Ref. 13 in four different forms. They describe the relationships of the six strains, six stresses, three electric displacements, and three electric fields at any time and at any point in the piezoelectric material. A piezoelectric material is anisotropic, with the constitutive conditions depending on its polarization direction.

The piezoceramics are plated with electrodes on the surfaces whose outer normal directions are parallel to the z axis. For the electrical components, only E_3 and D_3 exist. Since the piezoelectric strut is designed to carry load in the axial direction, only T_3 and S_3 in the z direction are considered. To model the active structure with known applied forces and electric voltages, it is necessary to choose the mechanical displacement and electric displacement as the independent variables. To this end, the constitutive equations to be used are

$$T_3 = c_{33}^D S_3 - h_{33} D_3 \tag{1a}$$

$$E_3 = -h_{33} S_3 + \beta_{33}^S D_3 \tag{1b}$$

System-Governing Equations

The truss structure is naturally modeled by finite elements. Let the displacement in the element be approximated by a linear shape function as

$$w(z,t) = \begin{bmatrix} 1 - \dfrac{z}{L} & \dfrac{z}{L} \end{bmatrix} \begin{Bmatrix} w_1(t) \\ w_2(t) \end{Bmatrix} \tag{2}$$

Then the strain derived from the strain-displacement relationship is

$$S_3(t) \equiv w_{,z}(z,t) = \begin{bmatrix} -\dfrac{1}{L} & \dfrac{1}{L} \end{bmatrix} \begin{Bmatrix} w_1(t) \\ w_2(t) \end{Bmatrix} \tag{3}$$

The internal energy including elastic, mutual, and dielectric energies is

$$\begin{aligned} V &= \int \left(\tfrac{1}{2} c_{33}^D w_{,z}^2 - h_{33} w_{,z} D_3 + \tfrac{1}{2} \beta_{33}^S D_3^2 \right) \mathrm{d}\Omega \\ &= \sum_i \left[\frac{1}{2} \left(\frac{c_{33}^D A}{L} \right)_i \begin{bmatrix} w_1 & w_2 \end{bmatrix}_i \begin{bmatrix} 1 & -1 \\ -1 & 1 \end{bmatrix} \begin{Bmatrix} w_1 \\ w_2 \end{Bmatrix}_i \right. \\ &\quad \left. - \frac{h_{33i}}{n} Q_{3i} \begin{bmatrix} -1 & 1 \end{bmatrix} \begin{Bmatrix} w_1 \\ w_2 \end{Bmatrix}_i + \frac{1}{2} \left(\frac{\beta_{33}^S}{nA} \right)_i Q_{3i}^2 \right] \end{aligned} \tag{4}$$

where the volume integration is carried over the entire structure and the summation over the number of structural elements. The kinetic energy is

$$\begin{aligned} T &= \int \frac{1}{2} \rho \dot{w}^2 \, \mathrm{d}\Omega \\ &= \sum_i \frac{1}{2} \left(\frac{mL}{6} \right)_i \begin{bmatrix} \dot{w}_1 & \dot{w}_2 \end{bmatrix}_i \begin{bmatrix} 2 & 1 \\ 1 & 2 \end{bmatrix} \begin{Bmatrix} \dot{w}_1 \\ \dot{w}_2 \end{Bmatrix}_i \end{aligned} \tag{5}$$

The work done by the applied forces and voltage is

$$W = \sum_i \left(\bar{N}_1 w_1 + \bar{N}_2 w_2 + n \int \bar{V}_3 D_3 \, dA \right)_i$$

$$= \sum_i (\bar{N}_1 w_1 + \bar{N}_2 w_2 + \bar{V}_3 Q_3)_i \tag{6}$$

A variational principle may be expressed as

$$\delta \int_{t_1}^{t_2} (T - V + W) \, dt = 0 \tag{7}$$

The governing equations in an element derived from the variational principle are

$$\frac{mL}{6}\begin{bmatrix} 2 & 1 \\ 1 & 2 \end{bmatrix}\begin{Bmatrix} \ddot{w}_1 \\ \ddot{w}_2 \end{Bmatrix} + \frac{c_{33}^D A}{L}\begin{bmatrix} 1 & -1 \\ -1 & 1 \end{bmatrix}\begin{Bmatrix} w_1 \\ w_2 \end{Bmatrix} - \frac{h_{33}}{n}\begin{bmatrix} -1 \\ 1 \end{bmatrix} Q_3 = \begin{Bmatrix} \bar{N}_1 \\ \bar{N}_2 \end{Bmatrix} \tag{8a}$$

$$-\frac{h_{33}}{n}[-1 \quad 1]\begin{Bmatrix} w_1 \\ w_2 \end{Bmatrix} + \frac{\beta_{33}^S d}{nA} Q_3 = \bar{V}_3 \tag{8b}$$

Since Eq. (8b) is an algebraic equation, one can solve for Q_3 in terms of w_1 and w_2 and then substitute back into Eq. (8a). The governing equations in an element are then

$$\frac{mL}{6}\begin{bmatrix} 2 & 1 \\ 1 & 2 \end{bmatrix}\begin{Bmatrix} \ddot{w}_1 \\ \ddot{w}_2 \end{Bmatrix} + \frac{c_{33}^E A}{L}\begin{bmatrix} 1 & -1 \\ -1 & 1 \end{bmatrix}\begin{Bmatrix} w_1 \\ w_2 \end{Bmatrix} = \begin{Bmatrix} \bar{N}_1 - \dfrac{e_{33}A}{d}\bar{V}_3 \\ \bar{N}_1 - \dfrac{e_{33}A}{d}\bar{V}_3 \end{Bmatrix} \tag{9a}$$

$$Q_3 - \frac{e_{33}A}{d}[-1 \quad 1]\begin{Bmatrix} w_1 \\ w_2 \end{Bmatrix} = C^S \bar{V}_3 \tag{9b}$$

Note that the forces applied to the structure at the nodal points by the piezoelectric strut are equivalent to two axial forces of opposite sign. Once the w_1 and w_2 are solved from Eq. (9a), the electric charge can be obtained from Eq. (9b) and the rest of the variables from the constitutive equations. For a piezoelectric strut connected to a power amplifier, which is a voltage source, the applied voltage is known, and one can use Eqs. (9a) and (9b) to solve for w_1, w_2, and Q_3. When a piezoelectric material is used as a rate sensor, it is connected to a current amplifier. In this case, the input terminals of the current amplifier are virtually grounded, which means the input voltage to the piezoelectric sensor is almost zero. Therefore, the above governing equations work equally well for a piezoelectric actuator or a piezoelectric sensor if the piezoelectric material meets the constitutive conditions described in Eq. (1).

For our case, $\bar{N}_1$ and $\bar{N}_2$ were zero, and the values for $c_{33}^E A/L$ were 0.7995×10^6 and 1.1992×10^6 lb/in. for the diagonal and longeron piezoelectric struts, respectively. The value for $e_{33}A/d$ was 1.888 lb/volt for both the diagonal and longeron piezoelectric struts.

Sensing

In this study, PVDF films are used as piezoelectric sensors. The film is thin and flexible, and it can be easily wrapped on an element of the structure. Its stiffness is negligible, and its electric field is almost zero when a current amplifier is used. To be used as a sensor, e_{31} is used. For a piezoelectric film wrapped on a cylindrical element of the structure, its poling direction is in the radial direction. The constitutive equations for the piezoelectric film, in cylindrical coordinates, are

$$T_3 = c_{33}^D S_3 - h_{r3} D_r \tag{10a}$$

$$E_r = -h_{r3} S_3 + \beta_{rr}^S D_r \tag{10b}$$

As described earlier, when a current amplifier is connected to a piezoelectric film, the electric field in the piezoelectric film is almost zero. From Eq. (9b), with proper coefficients, the electric charge on a piezoelectric film is

$$Q_r = \frac{e_{r3} A_s}{L_f}(w_2 - w_1) \tag{11}$$

Since the current $i = dQ_r/dt$, the signal measured from a piezoelectric film and current amplifier is

$$y = \frac{e_{r3} A_s Z}{L_f}[-1 \quad 1]\begin{Bmatrix} \dot{w}_1 \\ \dot{w}_2 \end{Bmatrix} \tag{12}$$

The above equation indicates that the piezoelectric film incorporated with a current amplifier measures the relative velocity. If the film is small in comparison to the structural member, it measures strain rate. But if the film is large with respect to the structural member, it is more precise saying that a piezoelectric film with a current amplifier measures relative velocity. If the strain is uniform in a structural member, the relative velocity differs from the strain rate by a scalar factor of the length of the piezoelectric film. Direct-rate feedback can be implemented by using a collocated piezoelectric film and piezoelectric strut as the control sensor and actuator, respectively.

Rate Feedback Control

Assuming viscous damping, from Eq. (9a), the equation of motion of the global structure can be rewritten as

$$\boldsymbol{M}\ddot{\boldsymbol{x}} + \boldsymbol{D}\dot{\boldsymbol{x}} + \boldsymbol{K}\boldsymbol{x} = \boldsymbol{B}_1 \boldsymbol{f} + \boldsymbol{B}_2 \boldsymbol{u} \tag{13}$$

The outputs of displacement, velocity, and acceleration may be expressed as

$$\boldsymbol{y} = \boldsymbol{C}_1 \boldsymbol{x} + \boldsymbol{C}_2 \dot{\boldsymbol{x}} + \boldsymbol{C}_3 \ddot{\boldsymbol{x}} \tag{14}$$

Collocation of actuator and sensor pair means that the output influence matrix is the transpose of the input influence matrix with a difference of a scalar factor only, i.e., $\boldsymbol{C} = \alpha \boldsymbol{B}^T$. To study the stability of the closed-loop system, there is no loss of generality to set $\boldsymbol{f}$ to be zero. The direct rate feedback implies that $\boldsymbol{u} = -\boldsymbol{G}\boldsymbol{C}_2\dot{\boldsymbol{x}} = -\boldsymbol{G}\alpha\boldsymbol{B}_2^T\dot{\boldsymbol{x}}$.

$$\boldsymbol{M}\ddot{\boldsymbol{x}} + (\boldsymbol{D} + \boldsymbol{B}_2\boldsymbol{G}\alpha\boldsymbol{B}_2^T)\dot{\boldsymbol{x}} + \boldsymbol{K}\boldsymbol{x} = \boldsymbol{0} \tag{15}$$

When the damping matrix of the closed-loop system, $\boldsymbol{D} + \boldsymbol{B}_2\boldsymbol{G}\alpha\boldsymbol{B}_2^T$, is positive definite, the closed-loop system is guaranteed to be stable.[14]

Testbed Description

Figure 1 is an illustration of the Tenbay truss test article showing the sensor and piezoelectric strut actuator locations. The truss has a total of 10 bays, with each bay consisting of a 10-in. cube. It is in an inverted-L shape, with 2 bays cantilevered horizontally from a base plate and 8 bays extending vertically downward. The individual struts are made of aluminum, as are the corner ball joints connecting each bay. Threaded steel rods are used to secure the struts to the ball joints. In addition, six steel bars of 7 lb each are mounted on the lower truss battens, three on each side, to lower the first two natural frequencies below 10 Hz.

Two commercial piezoelectric struts (Physik Instrumente[15]) are mounted in the truss bay closest to the support—one as the lower horizontal member (longeron strut) and one as the adjacent diagonal member (diagonal strut). Figure 2 shows a schematic of the commercial piezoelectric actuator, indicating the primary parts. These actuators take the place of the nominal struts, with steel support studs fabricated to connect the piezoelectric struts to the ball joints. The chosen locations correspond to those determined by a finite element model (FEM) of the truss to have the highest strain energy. Basic information on these actuators are given in Table 1.[15]

Instrumentation consists of a strain gage and a piezoelectric film mounted on opposite ends of each actuator. An additional piezoelectric film sensor and strain gage are placed on the diagonal strut in the truss bay face directly opposite to the face containing the

Table 1 Piezoelectric strut actuator data

Strut parameter	Longeron strut	Diagonal strut
Model number	P243.30	P243.40
Expansion at −1000 V, μm	40	60
Maximum pushing force, lb	6750	6750
Stiffness, lb/in.	1.1992×10^6	0.7995×10^6
Total length, in.	4.58	5.67
Weight, lb	2.75	3.25
Resonant frequency, Hz	4500	2200

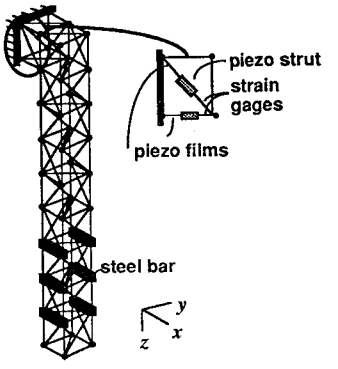

Fig. 1 Schematic of Tenbay structure.

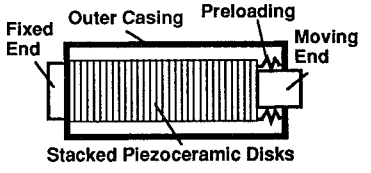

Fig. 2 Schematic of piezoelectric actuator.

piezoelectric struts. The two piezoelectric strut actuators are driven by a two-channel model 50/750 high-voltage power amplifier, from Trek, Inc. (Medina, NY), capable of producing alternating-current (AC) voltages of up to −1500 V at an average current level of 50 mA. For this study, the piezoelectric struts are biased by a negative direct-current (DC) voltage with an AC dynamic signal superimposed. Separate current amplifiers convert the current collected by the individual piezoelectric films to voltage outputs. This instrumentation is interfaced to a computer-automated measurement and control (CAMAC) rack, which performs the analog-to-digital (A/D) and the digital-to-analog (D/A) conversions and the analog filtering of the sensor signals. A VAX 3200 workstation is used for real-time control tests. A GenRad 2515 is also used for frequency response measurements.

Modeling Issues

An initial FEM analysis based on Eq. (9a) was performed using MSC/NASTRAN. Both piezoelectric struts and their respective supporting studs were modeled as single rods. The stiffnesses of the two piezoelectric struts, which includes the connecting support studs and the joint balls on either end, were previously measured and incorporated into the FEM. From this a linear reduced-order state-space model of the truss was developed. The first six vibrational mode shapes were used in the reduced model.

The frequency response function (FRF) between the output of the strain gage located on the diagonal strut on the opposite bay face to the input of the diagonal piezoelectric strut is shown in Fig. 3. As can be seen in the plots, the computed transfer function for this strain gage matches very well that measured in the laboratory. The phase discrepancy is attributed to the dynamics associated with either the high-voltage amplifier of the piezoelectric strut or the signal conditioner used for the strain gage or to some combination thereof. Neither the piezoelectric strut amplifier nor the signal conditioner dynamics is accounted for in the six-mode model. Similar results can be observed in Fig. 4, the FRF for the piezoelectric film sensor again located on the opposite side diagonal. These two measurements are not completely independent, but differ by a scalar factor of $j\omega$. This is expected since the strain gage senses in terms of relative displacement, whereas the piezoelectric film senses relative velocity. These results indicate that this six-mode model has fairly good global accuracy.

Larger errors are seen in the computed transfer functions of the strain gage and piezoelectric film sensors situated in the same truss face as the piezoelectric struts. These modeling errors are attributed to the strong local strain effects caused by the two piezoelectric struts. The local dynamics are not captured by the six-mode linear model. Numerical results indicated that increasing the grid points in the FEM or the number of vibrational modes in the model reduction did not improve the test and analysis correlation. To account for the local effects, the six-mode linear model, derived from the first six vibrational modes, was augmented with two static mode shapes. In addition, nodes were introduced between the piezoelectric struts and their connecting support studs in the FEM. This augmentation is outlined briefly below.

The basic idea behind this augmentation is to obtain a reduced set of basis vectors (some combination of static shapes and a small set of vibrational mode shapes) to describe the model, as opposed to relying solely on the vibrational modes. Previous work[16] has shown that in order to achieve similar local model fidelity, a model based on only vibrational modes would require a much larger set of basis vectors as compared to the model using combined vibrational and static vectors. The matrix of basis vectors, Φ, containing ϕ_{vi}, $i = 1, \ldots, 6$, and ϕ_{Si}, $i = 1, 2$, is defined as follows:

$$\Phi = [\phi_{v1} \quad \cdots \quad \phi_{v6} \quad \phi_{s1} \quad \phi_{s2}]. \tag{16}$$

Each static vector is a scaled displacement shape caused by a pair of unity force inputs by a piezoelectric strut. For scaling purposes, all eight mode shapes in Φ were scaled such that the maximum values were unity. Using Φ in the standard manner to reduce the full-order FEM into a lower order model and then converting into a first-order state-space model results in

$$\begin{Bmatrix} \dot{r} \\ \ddot{r} \end{Bmatrix} = \begin{bmatrix} 0 & I \\ -\hat{M}^{-1}\hat{K} & -\hat{M}^{-1}\hat{D} \end{bmatrix} \begin{Bmatrix} r \\ \dot{r} \end{Bmatrix} + \begin{bmatrix} 0 \\ \hat{M}^{-1}\hat{B}_2 \end{bmatrix} u \tag{17}$$

where $x = \Phi_r, \hat{M} = \Phi^T M \Phi, \hat{K} = \Phi^T K \Phi, \hat{D} = \Phi^T D \Phi$, and $\hat{B}_2 = \Phi^T B_2$.

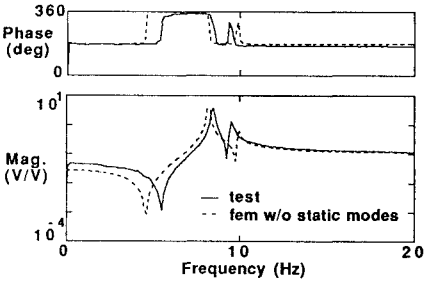

Fig. 3 FRFs of opposite diagonal strain gage to diagonal piezoelectric strut: test and FEM.

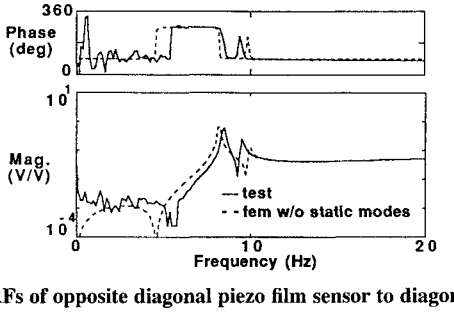

Fig. 4 FRFs of opposite diagonal piezo film sensor to diagonal piezoelectric strut: test and FEM.

The output equation [Eq. (14)] is transformed in a similar fashion, yielding

$$y = [\hat{C}_1 - \hat{C}_3\hat{M}^{-1}\hat{K} \quad \hat{C}_2 - \hat{C}_3\hat{M}^{-1}\hat{D}]\begin{Bmatrix} r \\ \dot{r} \end{Bmatrix} + \hat{C}_3\hat{M}^{-1}\hat{B}_2 u \quad (18)$$

where $\hat{C}_1 = C_1\Phi$, $\hat{C}_2 = C_2\Phi$, $\hat{C}_3 = C_3\Phi$.

In addition to the augmentation with the static mode shapes, a node was added to each connection point between the piezoelectric struts and their support studs, thus treating the piezoelectric struts and support studs as separate elements.

Figure 5 shows the FRFs between the collocated piezoelectric film output and the diagonal piezoelectric strut input from the two FEMs and are overlaid with the test data. The original FEM misses the zero at 5 Hz and shifted the zero at 42 Hz to around 11 Hz, which gives completely different characteristics from that of the test structure. In contrast, the augmented model shows a marked improvement in tracking the poles, zeros, and phase of the test results.

Control Test Results

Several real-time control laws, programmed on the VAX 3200 workstation, were executed on the Tenbay truss. The results of three of these controller tests, designed to suppress the vibrational motions of the truss, are presented in this section. The test procedures for all three controllers were the same, and they were as follows. Starting from rest, the truss was driven with sinusoidal inputs from the diagonal (excitation frequency 8.4 Hz) and longeron (excitation frequency 9.5 Hz) piezoelectric struts for 4.5 s in order to excite the first two modes. After 4.5 s, the excitation ceased, and either free decay was allowed for the open-loop case or the controller turned on for the closed-loop case. Figure 6 is an overall block diagram of Tenbay structure with a controller in closed loop. The top two blocks represent the piezoelectric strut power amplifiers and the Tenbay truss structure with the installed piezoelectric struts, respectively, the controller block containing specific control laws, which compute the commands to the piezoelectric strut power amplifiers. A DC bias was added to the control commands to the piezoelectric struts. The control laws are described in more detail below. For comparison purposes, Fig. 7 shows test and simulated time histories of the diagonal strain gage output for the open-loop system. The measured open-loop damping for the two modes was 0.18 and 0.4%, respectively.

The first controller was an LQG design. The LQG controller design is a model-based technique. For this particular controller, a system identification model was used before an FEM could be designed at the early stage of this study. The design procedure entailed the following: three 30-s data sets were obtained. Each set was formed from two random excitations (filtered below 15 Hz) into the piezoelectric struts, and the outputs were the two strain gage measurements. The sampling rate was 250 Hz. Using the system identification method of Ref. 17, a discrete 40-state, two-input, two-output model containing the first two modes with observer was obtained. The 40-state model was then reduced to 10 states based on the balanced model reduction techniques. Equation (19) is the form of the control law in the controller block:

$$\begin{aligned} x_c(k+1) &= A_c x_c(k) + B_c y(k) \\ u_c(k+1) &= C_c x_c(k) + D_c y(k) \end{aligned} \quad (19)$$

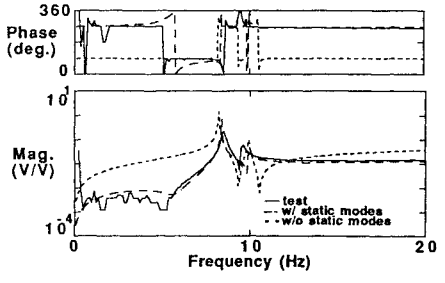

Fig. 5 FRFs and FEMs with and without static modes as compared to test data.

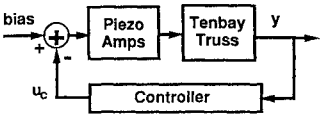

Fig. 6 Control feedback block diagram.

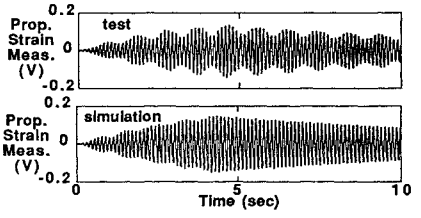

Fig. 7 Open-loop diagonal strain gage output time histories: test and simulation.

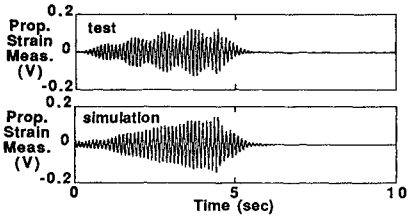

Fig. 8 LQG control diagram strain gage output time histories: test and simulation.

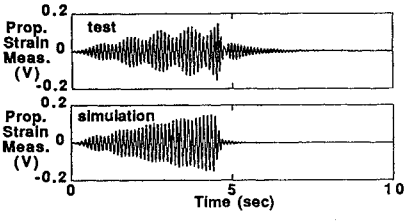

Fig. 9 Second-order decentralized control diagonal strain gage output time histories: test and simulation.

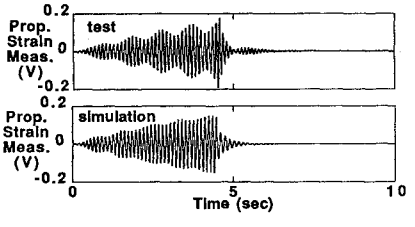

Fig. 10 Direct-rate feedback control diagonal strain gage output time histories: test and simulation.

The control law was discretized at 250 Hz, and the strain gage outputs were the sensor signals used in the controller. Figure 8 shows test and simulated diagonal strain gage sensor output time histories taken from this controller test. For this control test, the closed-loop damping of the two targeted modes was increased to 7.25 and 6.7, respectively.

The second controller is a second-order decentralized controller. The controller digitally simulates a second-order spring-mass-damper system attached to the structure to be controlled.[18] A collocated sensor/actuator provides the necessary temporal phase shift to effectively damp out the vibration using strain measurement. The controller was designed as single-input, single-output for each mode at each sensor/actuator pair. The control law equations were similar in format to those in Eq. (19). Figure 9 shows the test and simulated diagonal strain gage output time histories for the second-order decentralized controller test.

The third controller involved a simple output feedback design using the direct feedback of the relative velocity signals, measured

from the two piezoelectric film sensors mounted in series with the piezoelectric struts. Equation (20) shows the simple form of this control law:

$$u_c(k+1) = \alpha y(k) \tag{20}$$

Figure 10 shows the test and simulated diagonal strain gage output time histories for this test.

Note that all the simulations were calculated based on the modified FEM except for the LQG closed-loop case. The augmented linear model contained artificially high frequencies (on the order of kilohertz), associated with the static vectors. These high frequencies posed some problems in running the linear simulations. The "beating" is not seen on the simulation because the driving frequencies are not exactly matched with the natural frequencies of the FEM. The simulation and test data show the same envelope.

Conclusion

In this paper, an active truss structure using piezoelectric struts was modelled and tested. Although a reduced FEM derived from vibrational modes predicted the global model accurately, the forces applied by the piezoelectric struts introduced significantly local effects to the elements on and adjacent to the piezoelectric struts. Numerical results indicated that moderately increasing either vibrational modes or nodal points did not improve the ability of the reduced model to predict the local vibrations. Combining two static modes with only a few vibrational modes improved the matching of the reduced FEM to the test results. LQG, second-order decentralized, and direct rate feedback control schemes were designed and implemented successfully using a real-time VAX 3200 workstation. Simulation with the static mode modified state-space model showed good predictions of the measured closed-loop response.

There is a price to pay by including two static modes in the model. The artificial high frequency associated with the static mode shapes caused some difficulty in the simulation process. For a large space structure with highly distributed active members, more difficulty due to those fictitious high frequencies is foreseeable. More work in this area is warranted.

Acknowledgment

The authors express their appreciation to Jim Bailey of LESC for providing the MSC/NASTRAN finite element numerical model.

References

[1]Achenbach, J. D., *Wave Propagation in Elastic Solids*, North-Holland, Amsterdam, 1973.

[2]Kittel, C., *Introduction to Solid State Physics*, 6th ed., Wiley, New York, 1986.

[3]Holland, R., and Eer Nisse, E. P., "Variational Evaluation of Admittances of Multielectroded Three-Dimensional Piezoelectric Structures," *IEEE Transactions on Sonics and Ultrasonics*, Vol. SU-15, No. 2, 1968, pp. 119–132.

[4]Tiersten, H. F., *Linear Piezoelectric Plate Vibrations*, Plenum, New York, 1969.

[5]Ha, S.-K., Keilers, C., and Chang, F.-K., "Analysis of Laminated Composites Containing Distributed Piezoelectric Ceramics," *Journal of Intelligent Material Systems and Structures*, Vol. 2, No. 1, January 1991, pp. 59–71.

[6]Hagood, N. W., Chung, W. H., and von Flotow, A., "Modelling of Piezoelectric Actuator Dynamics for Active Structural Control," *Proceedings of the 31st Structures, Structural Dynamics, and Materials Conference*, Pt. 4 (Long Beach, CA), AIAA, Washington, DC, 1990, pp. 2242–2256.

[7]Won, C. C., "Active Control of Smart Structures," Ph.D. Dissertation, Georgia Inst. of Technology, Atlanta, GA, Dec. 1990.

[8]Won, C. C., "Vibration Control Structure Interaction in Adaptive Structures," *Proceedings of the Society for Experimental Mechanics 1991 Spring Conference*, Milwaukee, WI, June 1991, pp. 485–492.

[9]Lee, C.-K., and O'Sullivan, T. C., "Piezoelectric Strain Rate Gages," *Journal of the Acoustical Society of America*, Vol. 90, Supplement 2, Aug. 1991, pp. 945–953.

[10]Lee, C.-K., O'Sullivan, T. C., and Chiang, W.-W., "Piezoelectric Strain Rate Sensor and Actuator Designs for Active Vibration Control," *Proceedings of the AIAA 32nd Structures, Structural Dynamics, and Materials Conference*, Pt. 3 (Baltimore, MD), AIAA, Washington, DC, 1991, pp. 2197–2207.

[11]Obal, M. W., "Vibration Control of Flexible Structures Using Piezoelectric Devices as Sensors and Actuators," Ph.D. Dissertation, Georgia Inst. of Technology, Atlanta, GA, Sept. 1986.

[12]Won, C. C., Juang, J. N., and Lee, C. K., "Shear Strain Rate Measurement Applied to Vibration Control of High-Rise Buildings," *Proceedings of the International Workshop on Intelligent Structures*, Taipei, Taiwan, July 1990, pp. 299–311.

[13]Mason, W. P. (ed.), *Physical Acoustics*, Vol. 1, Part A, Academic, New York, 1964.

[14]Juang, J.-N., and Phan, M., "Robust Controller Designs for Second-Order Dynamic Systems: A Virtual Passive Approach," *Proceedings of the AIAA 32nd Structures, Structural Dynamics, and Materials Conference*, Pt. 3 (Baltimore, MD), AIAA, Washington, DC, 1991, pp. 1796–1805.

[15]*Physik Instrumente Catalog*, GmbH & Co., Waldbronn, Germany.

[16]Sandridge, C. A., and Haftka, R. T., "Modal Truncation, Ritz Vectors, and Derivatives of Closed-Loop Damping Ratios," *Journal of Guidance, Control, and Dynamics*, Vol. 14, No. 4, 1991, pp. 785–790 .

[17]Horta, L. G., Phan, M., Juang, J.-N., Longman, R. W., and Sulla, J., "Frequency Weighted System Identification and Linear Quadratic Controller Design," *Proceedings of the AIAA Guidance, Navigation, and Control Conference* (New Orleans, LA), AIAA, Washington, DC, 1991, pp. 1172–1179.

[18]Bruner, A. M., Belvin, W. K., Horta, L. G., and Juang, J.-N., "Active Vibration Absorber for the CSI Evolutionary Model: Design and Experimental Results," *Proceedings of the AIAA 32nd Structures, Structural Dynamics, and Materials Conference*, Pt. 4 (Baltimore, MD), AIAA, Washington, DC, 1991, pp. 2928–2938.